DOI 10.5162/Ultrasonic2025/P1.18

Preliminary Study on Muscular Tissue Characterization Using Continuous Shear Wave Elastography

Marie Tabaru[1], Naoki Tano[1], Toru Ogawa[2], Ren Koda[3], and Yoshiki Yamakoshi[3]
[1] Institute of Science Tokyo, 4259 Nagatsuta-cho, Midori-ku, Yokohama, Kanagawa, 226-8503, Japan
[2] Tohoku University Hospital, 1-1 Seiryo-machi, Aoba-ku, Sendai, Miyagi, 980-8574, Japan
[2] Gunma University, 1-5-1 Tenjin-cho, Kiryu, Gunma, 376-0052, Japan
tabaru.m.ab@m.titech.ac.jp

Abstract: There is a need for methods to assess muscle elasticity considering tissue inhomogeneity and heterogeneity. This study investigated shear wave morphology in muscle tissue during continuous shear wave elastography. Shear wave velocity, direction, and attenuation were measured in beef, pork, and chicken. Even when velocities were similar, attenuation and direction differed with fat and fibrotic content. These results support the feasibility of using this technique to assess muscle elasticity considering tissue inhomogeneity and heterogeneity.

Keywords: shear wave elastography, muscular characterization, heterogeneity, inhomogeneity, acoustic morphology

Introduction

In muscle tissue diagnosis using ultrasound elastography, there is a need for evaluation criteria that take into account the inhomogeneity and heterogeneity of muscle tissue [1, 2, 3]. For example, localized stiffness in the masseter muscle is a characteristic symptom of temporomandibular joint disorder. Since the internal structure of the masseter is more complex compared to other muscles, in clinical practice, palpation is used to assess tenderness related to stiffness, often employing the nine-part method [4]. Although there are studies on stiffness evaluation of the masseter muscle [5], the mechanism of its pathogenesis remains unclear. Drakonaki *et al.* reported that muscle elasticity images (i.e., color images) show the normal relaxed muscle as an inhomogeneous mosaic of intermediate stiffness. However, they do not yet understand what the color variation depends upon, and whether the color patterns are reproducible between different muscles and different individuals.

Meanwhile, continuous shear wave elastography (C-SWE), developed by the authors, utilizes an external mechanical vibrator to generate shear waves within biological tissue [6, 7, 8]. This vibrator induces microscale displacements in the tissue. The C-SWE technique reconstructs the excited shear waves, allowing for the visualization and assessment of muscle elasticity [9]. This study focused on observing the propagation characteristics of shear waves excited in C-SWE, investigating the inhomogeneity and heterogeneity of the muscle tissue. While morphological features in conventional ultrasound images have been widely used for disease diagnosis [10], here, we evaluate muscle tissue based on the morphological characteristics observed in shear wave imaging.

Measurement Method

In this study, five types of samples were prepared: chicken breast (CB), pork belly (PB), beef round (BR), pork tenderloin (PT), and beef tenderloin (BT), all purchased from a supermarket. Fig. 1(a) illustrates the experimental system setup to measure shear waves. An external mechanical vibrator was put on the surface of each sample, and shear waves were generated using the vibrator operating at 78 Hz. Shear wave measurements were conducted using a separate linear array ultrasound probe (Finggal Link, Japan; 128 active elements, frequency: 10 MHz) and a C-SWE system installed on a laptop computer [8]. B-mode image data and the real (I) and the imaginary (Q) signals (i.e., IQ signals) of the ROI (16×26 mm) were acquired by the C-SWE system.

Reconstruction Method of Shear Wave

Here, the reconstruction method of shear wave is described. The acquired IQ signals correspond to the Doppler signal, s, which is expressed as Eq. (1).

$$s = y_0 \exp(j\Delta\omega t), \tag{1}$$

where y_0 is the amplitude of the IQ signals. $\Delta\omega t$ is the phase component of the IQ signals. The Doppler phase shift is related to the displacement of the scatterer. Accordingly, the following relationship can be derived:

$$\Delta\omega t \propto u_0 \sin(2\pi f_s t + \Phi) \tag{2}$$

Here, u_0 is the amplitude of shear wave, f_s is the shear wave frequency, and Φ is the phase of shear

DOI 10.5162/Ultrasonic2025/P1.18

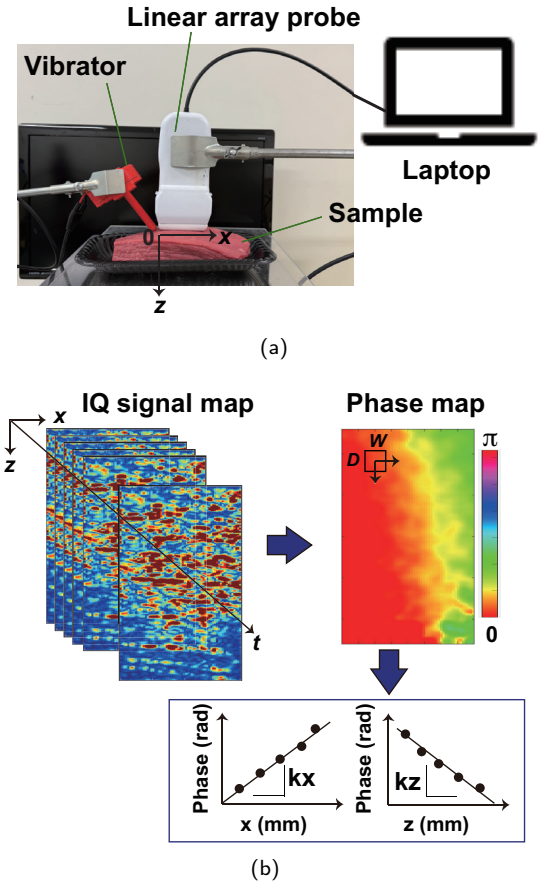

Fig. 1: (a) C-SWE experimental system and (b) flowchart of signal processing for shear wave reconstruction.

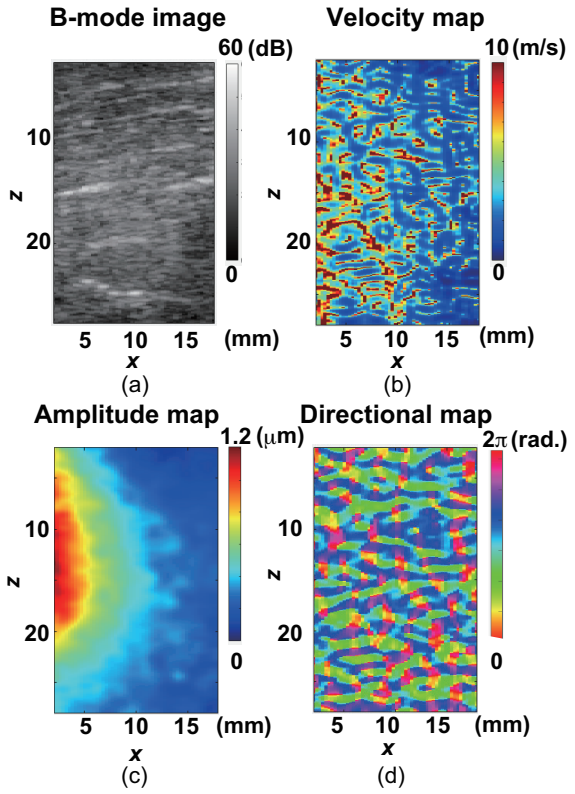

Fig. 2: Resultant images of BR sample. (a) B-mode image. (b) Velocity map. (c) Amplitude map. (d) Directional map.

wave. Therefore, by extracting the phase component of the IQ signals, the phase of shear wave is obtained. The wavenumbers, the shear wave velocity, and the shear wave propagation direction are calculated from Φ, which which is expressed as Eq. (3).

$$\Phi = k_x x + k_z z, \tag{3}$$

where k_x and k_z are the wavenumbers in the x and z directions, respectively. The wavenumbers of shear wave, the shear wave velocity, and shear wave propagation direction were calculated from Φ. k_x and k_z were calculated by Eqs. (4) and (5).

$$k_x = \frac{\partial \Phi}{\partial x} \tag{4}$$

$$k_z = \frac{\partial \Phi}{\partial z} \tag{5}$$

The shear wave velocity, v, was calculated by Eq. (6).

$$v = \frac{2\pi f_s}{\sqrt{k_x^2 + k_z^2}} \tag{6}$$

The shear wave propagation direction, dir, was calculated by Eq. (7).

$$dir = \arctan\left(\frac{k_x}{k_z}\right) \tag{7}$$

The amplitude of shear wave was also calculated from $|\Delta\omega t|$.

Fig. 1(b) illustrates the flowchart to calculate Φ and wavenumbers from IQ signals. In the experiment, a Φ was reconstructed by a signal processing method developed by the authors [8]. The phase signals inside the ROIs were divided into multiple sub-ROIs (D: 1.2 mm, W: 1.2 mm) and linear regression was performed to calculate the biaxial phase gradients in the sub-ROIs.

Results

Fig. 2 shows the B-mode image, the shear wave velocity map, the shear wave amplitude map, and the directional map of the BR sample. The vibration point is located approximately at $x = 0$ mm and shear wave propagates in the direction of $+x$. The resulting morphological characteristics of phase, velocity, amplitude, and direction reflect the properties of the muscle tissue. To evaluate the shear wave characteristics, we

DOI 10.5162/Ultrasonic2025/P1.18

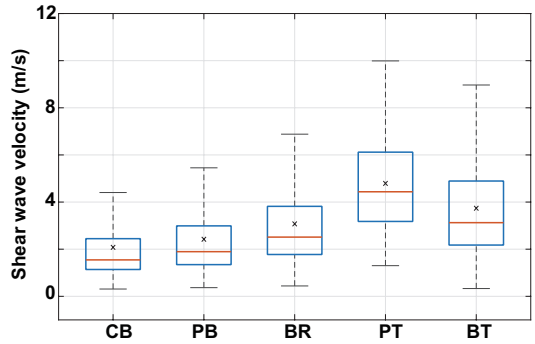

Fig. 3: Box plots of shear wave velocities. The 'x' symbol represents average values.

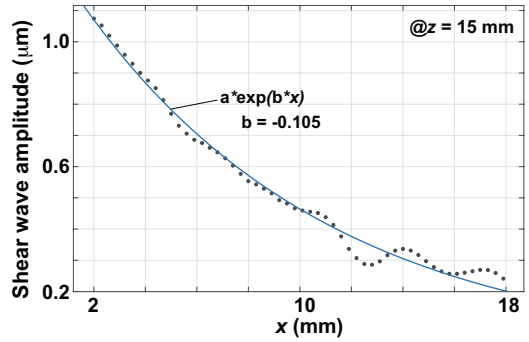

Fig. 4: Shear wave amplitude plot at $z = 15$ mm of BR sample and curve approximated by curve fitting method.

first consider the shear wave velocities. The calculated box plots are shown in Fig. 3. Here, velocities greater than 10 m/s were considered outliers. The velocities were 2.04 ± 1.52, 2.45 ± 1.67, 3.03 ± 1.84, 4.82 ± 2.04, and 3.45 ± 2.15 m/s for CB, PB, BR, PT, and BT, respectively. The velocities were within the range of the reference values [11]. CB and PB can be classified as samples with relatively slow shear wave velocities. On the other hand, PT and BT can be classified as samples with relatively fast shear wave velocities.

Second, the attenuation characteristics were investigated. As shown in Fig. 2 (c), the shear wave amplitude decreased as shear wave propagated. The attenuation coefficient, b, was calculated from the amplitude curve as shown in Fig. 4. Function, $a * \exp(b * x)$ is fitted to the attenuation curve by using Curve Fitting Toolbox (Matlab2025, MathWorks), where a is a real number. The b of BR was -0.105 (1/mm). The curve fit showed a high coefficient of determination of 0.98. Attenuation coefficients of CB, PB, BR, PT, and BT were -0.093, -0.170, -0.105, -0.065, and -0.064 (1/mm), respectively. The attenuation coefficient of pork belly was the highest. This is considered to be due to the high-fat content in pork belly.

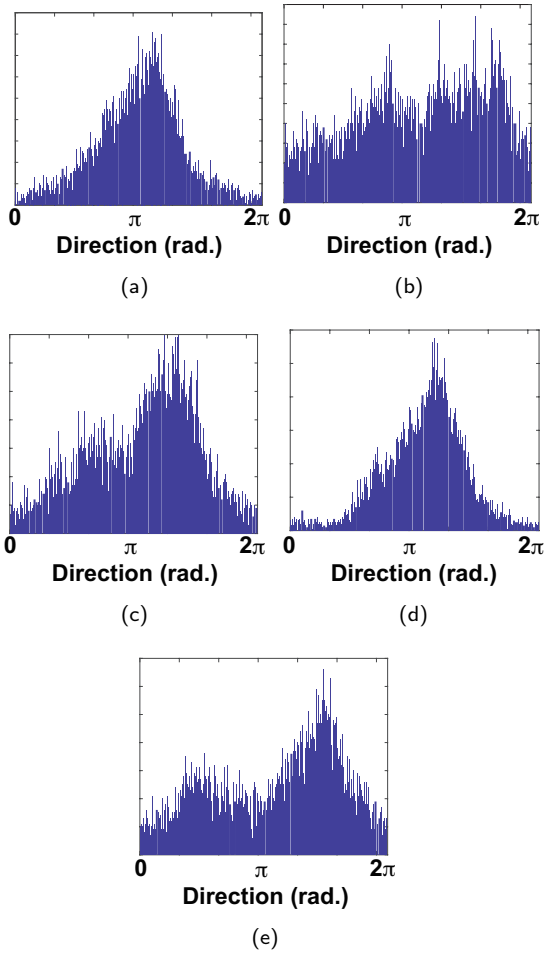

Fig. 5: Histogram of shear wave direction. π indicates that the propagation direction is horizontal. (a)CB. (b)PB. (c)BR. (d)PT. (e)BT.

Third, we investigate the propagation directions of shear wave. Fig. 5 shows the histograms of the directional maps. The directions of CB and PT are concentrated around π. This indicates that shear waves are propagating in the $+x$ direction. This observation indicates a high degree of structural homogeneity and alignment of the muscle fibers within the CB and PT regions. The directional variability observed in the PB region is presumably due to its heterogeneous structure, comprising both muscular and fat components. The wave propagation in the BR and BT regions exhibits components along the $+z$ axis, with a smaller proportion also oriented in the -z direction. This phenomenon is likely attributable to the inherent inhomogeneity in muscle structure and fiber orientation within the bovine tissue.

Discussion

First, we discuss the propagation direction of shear waves within muscle tissue. The variability in shear

wave direction is considered to be influenced by reflections occurring at muscle fibers, fat tissue, and fascial structures. This suggests that, in the future, directional variability of shear waves may enable the visualization of fibrosis — one of the parameters representing muscle inhomogeneity. However, further investigation using a physical simulation model is required. Next, we discuss the inhomogeneity and heterogeneity of muscle tissue. Skeletal muscle is composed of muscular tissue, fat components, and fibrous structures. In this study, an ex vivo feasibility study was conducted to explore the potential for evaluating tissue inhomogeneity and heterogeneity based on the direction and amplitude distribution of shear waves. In the future, quantitative evaluation using inhomogeneous or heterogeneous phantoms—with controlled fiber layering, density, and fiber orientation—along with the development of a corresponding physical model, will be necessary.

Conclusion

In this study, the inhomogeneity and heterogeneity of muscle tissue were evaluated based on the morphological characteristics observed in shear wave imaging. Shear wave velocity, propagation direction, and attenuation coefficient were measured in beef, pork, and chicken samples. Although the shear wave velocities were similar across samples, attenuation and directional characteristics varied depending on tissue composition, such as fat and fibrotic structures. These findings support the feasibility of using continuous shear wave elastography to assess muscle elasticity while accounting for tissue inhomogeneity and heterogeneity. As a future work, the evaluation of inhomogeneity and heterogeneity will be conducted using phantoms and simulations.

Acknowledgments

This work was supported in part by JSPS KAKENHI Grant Number 25K01237, the Cooperative Research Project of Research Center for Biomedical Engineering, and JKA's promotion funds from KEIRIN RACE.

References

[1] E. Drakonaki, G. Allen, and D. Wilson. "Ultrasound Elastography for Musculoskeletal Applications". In: *The British Journal of Radiology* 85.1019 (2012), pp. 1435–1445. DOI: 10.1259/bjr/93042867.

[2] D. Turo et al. "Novel Use of Ultrasound Elastography to Quantify Muscle Tissue Changes After Dry Needling of Myofascial Trigger Points in Patients With Chronic Myofascial Pain". In: *Journal of Ultrasound in Medicine* 34.12 (2015), pp. 2149–2161. DOI: 10.7863/ultra.14.08033.

[3] R. Sigrist et al. "Elastography: Review of Techniques and Clinical Applications". In: *Theranostics* 7.5 (2017), pp. 1303–1329. DOI: 10.7150/thno.18650.

[4] S. Beaumont et al. "Temporomandibular Disorder: a practical guide for dental practitioners in diagnosis and management". In: *Australian Dental Journal* 65.3 (2020), pp. 172–180. DOI: 10.1111/adj.12785.

[5] M. Takashima et al. "Quantitative Evaluation of Masseter Muscle Stiffness in Patients with Temporomandibular Disorders using Shear Wave Elastography". In: *Journal of Prosthodontic Research* 64.4 (2017), pp. 432–438. DOI: 10.1016/j.jpor.2017.01.003.

[6] Y. Yamakoshi et al. "Shear Wave Imaging of Breast Tissue by Color Doppler Shear Wave Elastography". In: *IEEE Transactions on Ultrasonics, Ferroelectrics, and Frequency Control* 64.2 (2017), pp. 340–348. DOI: 10.1109/TUFFC.2016.2626359.

[7] N. Tano et al. "Continuous Shear Wave Elastography for Liver Using Frame-to-Frame Equalization of Complex Amplitude". In: *Ultrasonic Imaging* 46.3 (2024), pp. 197–206. DOI: 10.1177/01617346241247127.

[8] R. Koda et al. "Application of Continuous Shear Wave Elastography Method with Multiple Frequency Selection to Liver Viscoelasticity Measurement". In: *Japanese Journal of Applied Physics* 63.4 (2024), 04SP82. DOI: 10.35848/1347-4065/ad3ae4.

[9] M. Tabaru et al. "Examination of Rapid Adjustment System Based on Screen Score Obtained using Continuous Shear Wave Elastography". In: *Journal of Medical Ultrasonics* 51.3 (2024), pp. 407–418. DOI: 10.1007/s10396-024-01439-7.

[10] S. Otsuka et al. "Investigation of the Association between Human Fascia Lata Thickness and its Neighboring Tissues' Morphology and Function using B-mode Ultrasonography". In: *Journal of anatomy* 239.5 (2021), pp. 1114–1122. DOI: 10.1111/joa.13505.

[11] L. S. Mikaela, A. M. Seyed, and A. M. Agur. "Measuring Shear Wave Velocity in Adult Skeletal Muscle with Ultrasound 2-D Shear Wave Elastography: A Scoping Review". In: *Ultrasound in Medicine & Biology* 49.6 (2023), pp. 1353–1362. DOI: 10.1016/j.ultrasmedbio.2023.02.005.